

## First-principle natural band alignment of GaN / dilute-As GaNAs alloy

Chee-Keong Tan and Nelson Tansu

Citation: *AIP Advances* **5**, 017129 (2015); doi: 10.1063/1.4906569

View online: <http://dx.doi.org/10.1063/1.4906569>

View Table of Contents: <http://scitation.aip.org/content/aip/journal/adva/5/1?ver=pdfcov>

Published by the *AIP Publishing*

---



# **Goodfellow**

metals • ceramics • polymers  
composites • compounds • glasses

**Save 5% • Buy online**  
70,000 products • Fast shipping

# First-principle natural band alignment of GaN / dilute-As GaNAs alloy

Chee-Keong Tan<sup>a</sup> and Nelson Tansu<sup>b</sup>

Center for Photonics and Nanoelectronics, Department of Electrical and Computer Engineering, Lehigh University, Bethlehem, PA 18015, USA

(Received 13 December 2014; accepted 13 January 2015; published online 22 January 2015)

Density functional theory (DFT) calculations with the local density approximation (LDA) functional are employed to investigate the band alignment of dilute-As GaNAs alloys with respect to the GaN alloy. Conduction and valence band positions of dilute-As GaNAs alloy with respect to the GaN alloy on an absolute energy scale are determined from the combination of bulk and surface DFT calculations. The resulting GaN / GaNAs conduction to valence band offset ratio is found as approximately 5:95. Our theoretical finding is in good agreement with experimental observation, indicating the upward movements of valence band at low-As content dilute-As GaNAs are mainly responsible for the drastic reduction of the GaN energy band gap. In addition, type-I band alignment of GaN / GaNAs is suggested as a reasonable approach for future device implementation with dilute-As GaNAs quantum well, and possible type-II quantum well active region can be formed by using InGaN / dilute-As GaNAs heterostructure. © 2015 Author(s). All article content, except where otherwise noted, is licensed under a Creative Commons Attribution 3.0 Unported License. [<http://dx.doi.org/10.1063/1.4906569>]

## I. INTRODUCTION

Owing to the desirable electronic and optoelectronic properties of nitride-based alloys, especially the direct and large band gap in the Brillouin Zone, rapid development of InGaN, AlGaIn and AlInN alloys have been witnessed in the past decade, leading to successful fabrication of LEDs operating in the blue-green light emitting diodes (LEDs).<sup>1-10</sup> While InGaN- and GaN-based alloys have been widely implemented into solid state lighting applications, the InGaAs- and GaAs-based alloys are established material systems for telecommunication and infrared device technologies.<sup>11,12</sup> The mixed AsN-based alloys had been studied in the dilute-nitrogen regime specifically for resulting in some of the breakthroughs in the long wavelength lasers on GaAs.<sup>13-18</sup> The findings of dilute-nitride GaAs-based alloy had led into the state-of-the-art and low threshold laser devices for the telecommunication applications.<sup>16-18</sup> In contrast to the successful development on dilute-nitride alloys – based on InGaAsN, the research on dilute-arsenic (As) GaNAs-based alloy is at the early stage. Dilute-arsenic GaNAs-based alloy has yet to be implemented into devices and the available literature published on this alloy subject is severely limited.<sup>5,19-28</sup>

Li and co-workers first succeeded in incorporating As into thin film GaN through metal-organic chemical vapor deposition (MOCVD), and the redshift of band gap energy of the dilute-As GaNAs alloy was observed in the photoluminescence study.<sup>5</sup> Further studies have also shown successful incorporation of As-content up to 7% into GaN material through MOCVD,<sup>20</sup> and synthesis of GaNAs alloy in full composition range through molecular beam epitaxy (MBE) was recently reported.<sup>21</sup> Recent experimental work by Yu et al reported that the band gap of dilute-As GaNAs alloy reaches  $2.3 \text{ eV} \pm 0.5 \text{ eV}$  at roughly 6%-As impurities incorporation.<sup>21</sup> Most recently, the electronic properties of the dilute-As GaNAs alloy was studied and it was suggested that the alloy potentially

<sup>a</sup>Electronic mail: [ckt209@lehigh.edu](mailto:ckt209@lehigh.edu)

<sup>b</sup>Electronic mail: [tansu@lehigh.edu](mailto:tansu@lehigh.edu)



has lower Auger recombination rate, which is essential to achieve suppression of Auger process at high current density.<sup>22</sup> These findings indicate that dilute-As GaNAs alloy as a promising material for visible light applications specifically for addressing the droop issue in LED technologies.

Nevertheless, in order to implement dilute-As GaNAs alloy in devices such as LEDs, semiconductor heterostructures between dilute-As GaNAs alloy and GaN alloy need to be formed. The understanding of the band discontinuities for two different III-V or III-Nitride materials is critical<sup>10,15,29–38</sup> for designing nanostructures or heterostructures applicable in device implementation. Up to today, there has been no comprehensive and conclusive study in predicting and determining the natural band alignment between GaN and dilute-As GaNAs alloy. Therefore the understanding of the band discontinuity of GaNAs / GaN will be essential for evaluating the optical and carrier transport properties in devices incorporating this heterostructure.

In this work, we present a comprehensive quantitative analysis of the relative natural band alignment of dilute-As GaNAs / GaN heterostructures using First-Principle method. We examine the natural band offsets of the strain-free dilute-As GaNAs alloy relative to the GaN alloy. In addition to that, we also discussed about the source of the drastic reduction of the band gap from analyzing the band offset between GaN and dilute-As GaNAs alloy, in which the upward movement of the valence band of the dilute-As GaNAs alloy was shown to contribute significantly to this effect. Our finding provides useful understanding of the band parameters important for enabling the implementation of dilute-As GaNAs alloy and heterostructures in GaN-based electronics and optoelectronics device technologies.

## II. COMPUTATIONAL METHOD

The determination of band offsets between two materials can be performed through the projected local density of states calculation (LDOS)<sup>29</sup> and also the potential line-up method.<sup>30,31</sup> While both methods are capable of providing insight on how the alignment between two materials should be, the potential line-up method is chosen in this work simply because the LDOS calculation requires higher demand of convergence parameters which were previously identified, resulting in a slower convergence compared to that of the charge density.<sup>32</sup> Note that the natural band alignment of the unstrained system (GaN / dilute-As GaNAs) is focused in our DFT calculation. The advantage of this alignment for a material system is that it can be directly connected to the physical situation of photoelectrode<sup>33,34</sup> and active regions for lasers or LEDs.<sup>27,28</sup> In the potential line-up method, the calculation of valence band offset (VBO) between two different materials is a combination of two terms which are the band structure term ( $\Delta E_v$ ) and the electrostatic term ( $\Delta V$ ). For the band structure term, it is defined as the difference between the top of the valence bands of two bulk materials with respect to the average electrostatic potential at core. The information of the valence bands of the bulk materials can be obtained from two independent standard bulk band structure calculations. For the electrostatic potential term, it is obtained from the lineup of the macroscopic average electrostatic potential in two material slabs, by aligning it with respect to the vacuum level in the slabs.<sup>33</sup>

Consequently, in our DFT analysis, two independent approaches were performed to obtain the valence band maximum (VBM) difference and the macroscopic potential difference between GaN and dilute-As GaNAs materials. The supercell approach was applied to build the appropriate crystal structure for the electronic properties calculation. The crystal structures of GaN and dilute-As GaNAs alloys were built using the atomistic simulation package MedeA-VASP.<sup>39</sup> Figure 1(a) and (b) show a constructed GaNAs alloy bulk and slab crystal structures consisting of a total of 32 atoms respectively. With one N atom being substituted by one As atom, the composition of the dilute-As GaNAs crystal structure is thus 6.25%-As. Similarly, bulk and slab structures with a total of 48 atoms can also be constructed with one As atom as the impurity in the system, leading to 4.17%-As GaNAs alloy. In addition, the slab structures for the dilute-As GaNAs and GaN in a repeated-slab geometry and nonpolar orientation are chosen in the calculation in order to negate the potential polarization field, which would affect the electrostatic potential in the structures.

Based on the constructed crystal structures of dilute-As GaNAs and GaN, the calculations of the bulk band structure and the electrostatic potential were then performed using MedeA-VASP

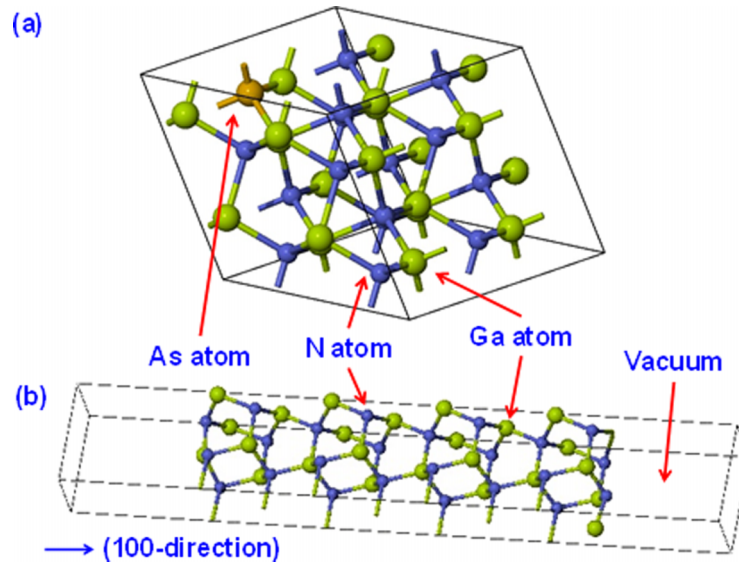


FIG. 1. (a) Supercell and (b) Slab of GaNAs alloy built using MedeA-VASP package. These 32-atom supercell consists of 16 Gallium (Ga) atoms, 15 Nitrogen (N) atoms and 1 Arsenic (As) atom, corresponding to 6.25% As-content in GaNAs alloy.

with projected augmented wave pseudopotentials (PAW) method implemented in the code.<sup>39</sup> Local density approximation (LDA) exchange-correlation potential was used in the DFT calculation.<sup>39,40</sup> The electronic wave functions are described in plane wave basis with the cutoff energy fixed at 400 eV. The structure optimization was performed by relaxing the atom positions with the Hellmann-Feynman force set to 0.02 eV/Å before the calculation takes place. The energy convergence tolerance was set at  $1 \times 10^{-5}$  eV/atom, while the external stress was set to 0 GPa. The Gamma-centered Monkhorst-Pack grid and high symmetry k-points were used for the band structure and the electrostatic potential calculations. Note that different Monkhorst-Pack k-point meshes were generated in the calculations attributed to the use of different supercell and slab sizes. The spin-orbit coupling was excluded in both calculations since the effect in the wide band gap III-nitride semiconductor is negligible. These parameters were consistently used in both supercell and slab approaches.

### III. RESULTS AND DISCUSSIONS

Figure 2 shows the computed planar average and macroscopic average of electrostatic potential energy within slabs consisting of layers of GaN and dilute-As GaNAs, as well as the vacuum region. As shown in figure 2, the planar average and macroscopic average electrostatic potential of the GaN and dilute-As GaNAs alloys were aligned by referencing it to the vacuum energy level respectively. In our study, the vacuum energy level was aligned as 0 eV simply to better represent the result. In addition, due to slight fluctuation of macroscopic average potential, the average of the macroscopic average potential of the GaN and dilute-As GaNAs alloy was obtained which is represented as a solid straight line as shown in figure 2. Two key factors need to be taken into consideration for analyzing the planar average and macroscopic average electrostatic potentials in DFT calculation. First, the interface between the GaN alloy or dilute-As GaNAs alloy and the vacuum results in the fluctuation of the planar average electrostatic potential. At some distances away from the interface, the planar average electrostatic potential was stabilized and this could be represented for the material.<sup>33</sup> Second, the As impurity existence in the dilute-As GaNAs slab results in the fluctuation of planar and macroscopic average around the impurity, due to the different charge density possessed by the different types of atoms.

Building on the computed result from band structure and macroscopic average electrostatic potential calculations, the VBO of GaN/dilute-As GaNAs material system is determined for various

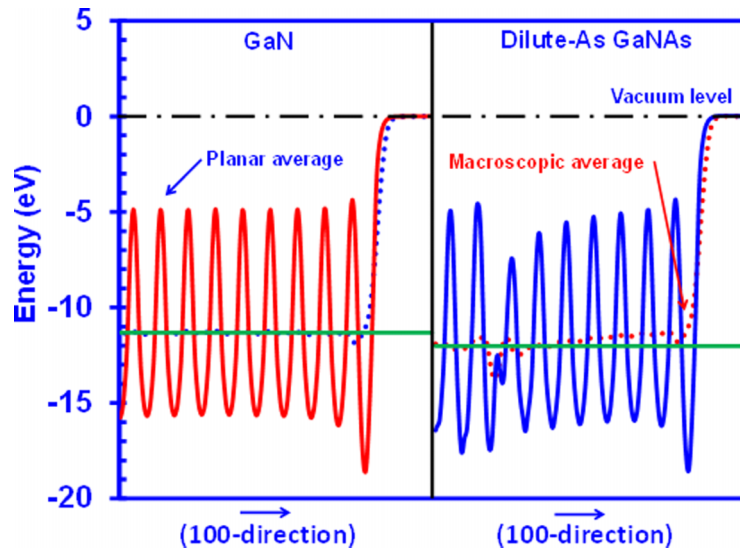


FIG. 2. The planar average (solid line) and the macroscopic average (dot line) of the electrostatic potential near the surface for GaN and dilute-As GaNAs alloys computed within the DFT-LDA functional. The vacuum level is aligned as 0 eV (dash line) as shown in the figure.

composition ranged from 0% up to 12.5%-As impurity. The conduction band position for GaN / dilute-As GaNAs were obtained by adding the experimental band gaps<sup>21</sup> onto the calculated valence band position, similar to the approaches reported by others.<sup>32,33,35,36,41</sup> This approach is commonly used in DFT calculation to avoid the band gap error originated from the LDA approximation.<sup>32,33,35,36,41</sup> Note that the natural  $\Delta E_v$  is found as insensitive between semiconductor systems with a common anion or cation and with the same crystal structure,<sup>36</sup> thus the use of LDA for the calculation for GaN and dilute-As GaNAs alloys is justified and should provide the necessary insight of how the  $\Delta E_v$  and  $\Delta E_c$  evolve with different As impurity composition of dilute-As GaNAs alloy.

Figure 3 shows the valence band and conduction band alignment of dilute-As GaNAs alloy with respect to the GaN as a function of As-composition up to 12.5%. As the GaN alloy is taken as a reference, its valence band position is presumed at 0 eV while its conduction band position is set at 3.4 eV, constituting 3.4 eV energy band gap. When As impurity is introduced into GaN, the conduction band position is lowered down from 3.4 eV at 0%-As GaNAs to 3.346 eV at 12.5%-As GaNAs, as shown in figure inset of figure 3. In our finding, the conduction band energy of dilute-As GaNAs alloy is reduced by approximately 55 meV over the studied composition range from 0% to 12.5%-As. The corresponding valence band position raises up from 0 eV for 0%-As GaNAs alloy up to 1.15 eV for 12.5%-As GaNAs alloy. Based on the experimental measurement on the MBE-grown GaNAs alloy, Yu and co-workers reported the valence band position for the dilute-As GaNAs alloy relative to GaN as  $0.8 \text{ eV} \pm 0.3 \text{ eV}$  from 2% to 10% of As-content in the alloy, and  $1 \text{ eV} \pm 0.3 \text{ eV}$  with roughly 17.5% of As-content in the alloy.<sup>21</sup> Our First-Principle findings are in reasonable agreement with the experimental data available in the literature.<sup>21</sup>

The discrepancies between our computed data and experimental results for the GaN / dilute-As GaNAs alloy could mainly be caused by the strain effect existing in the grown alloy due to the much larger atomic size of arsenic atom and also the formation of As-cluster and As-pair in the dilute-As GaNAs alloy. Note that our result is computed based on ideal and relaxed structure, and the polarization field effects as well as charge transfer issue at the interface between GaN and dilute-As GaNAs alloy are not taken into consideration.

As shown in figure 3, the valence band offset is significantly larger than the conduction band offset for the GaN / dilute-As GaNAs material system. The results (figure 3) for dilute-As GaNAs alloy exhibit very distinct corresponding properties as observed in the dilute-nitride GaAsN / GaAs heterostructures.<sup>15</sup> The incorporation of dilute amount of nitrogen (1-2%) in the GaAs or InGaAs

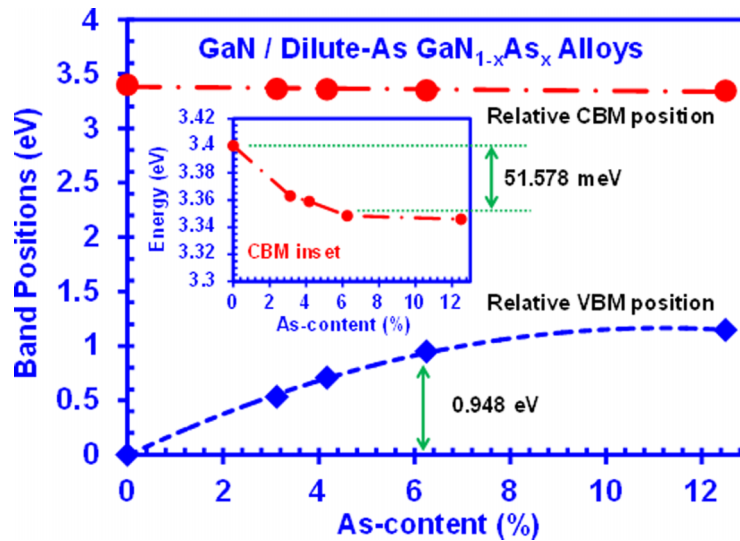


FIG. 3. VBM and CBM position of dilute-As GaNAs alloy relative to GaN as a function of arsenic content up to 12.5%. The figure inset shows the CBM position of dilute-As GaNAs alloy in a relatively smaller energy scale.

result in large bandgap reduction accompanied by a large conduction band offset ratio ( $\sim 80\%$ ).<sup>15</sup> The addition of nitrogen atoms in dilute amount into the GaAs or InGaAs alloy introduced the localized energy states near to the conduction band of the GaAs or InGaAs alloy, which in turn result in strong modification of the conduction band properties in the GaAsN or InGaAsN alloys strongly affected by the narrow resonant N energy states.

In dilute-As GaNAs alloy, the addition of As impurity in the GaN alloy results in the formation of localized As states about 0.4 eV above the valence band of GaN alloy.<sup>26</sup> Consequently, there is a strong interaction between the localized As states and the valence band states of GaN resulting in a strong modification in the valence band properties for the dilute-As GaNAs alloy. The conduction states of the dilute-As GaNAs alloy are however much less influenced since the position of the impurity level of the As-states is far away from the conduction band edge. This finding indicates that the valence band of the dilute-As GaNAs alloy is heavily perturbed by the As-impurity while conduction band is relatively less affected.

The understanding of the band offsets provides an intuitive insight into the source of the bandgap bowing.<sup>33</sup> In the case of GaN / dilute-As GaNAs heterojunction, the dominant valence band offsets strongly indicate the bandgap bowing as attributed to the upward movement of the valence band edge positions. The physical reason behind this finding can be explained due to the strong interactions of the localized As states and the valence band edge in GaN.

Figure 4 shows the VBO and CBO ratios as a function of arsenic composition up to 12.5% As-content for the GaN / dilute-As GaNAs material system. The VBO ratio is much higher than that of the CBO ratio in the GaN / dilute-As GaNAs material system. Overall, the VBO ratio can be approximated as 0.95, while the CBO ratio is relatively small at 0.05. The figure inset of the figure 4 shows that the VBO ratio has slight increment while CBO ratio has slight reduction over the composition range. This finding can be reasonably explained, as the increment of As percentage in the GaN results in stronger interaction between the localized states and its valence states. Based on this result and judging the trend of the CBO and VBO ratio values with respect to the As composition, the CBO : VBO ratio for dilute-As GaNAs can be taken as 5:95 for As-content up to 12.5%. The determination of the CBO and VBO ratios is essential for enabling proper design of this heterostructure in nanostructure and device applications.<sup>42</sup>

Prior works by MBE epitaxy have shown the challenges in obtaining crystalline form of dilute-As GaNAs for As-content above 25%.<sup>21</sup> Yu and co-workers showed that the XRD measurement on MBE-grown dilute-As GaNAs retains its crystallinity structure up to As-content of 17.5%, and higher As incorporation into the film results in amorphous structure attributed to the strong

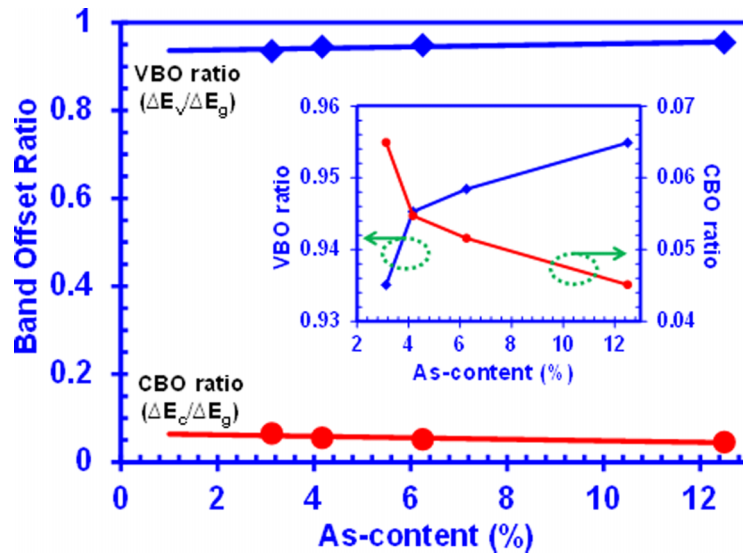


FIG. 4. The valence band offset (VBO) ratio and conduction band offset (CBO) ratio of the GaN / dilute-As GaNAs heterojunction as a function of arsenic content up to 12.5%-As.

clustering of As in the alloy. The crystallinity of the GaNAs alloy was only recovered in the regime of dilute-nitride GaNAs with N-content less than 15%.<sup>21</sup> As a result, the band offset ratio value of GaN / dilute-As GaNAs alloy should only be considered in the crystalline structure for As-content below 17.5%.

Our analysis indicates a type-I band alignment for GaN / dilute-As GaNAs heterojunction with As-content ranging from 0% up to 12.5%, as illustrated in figure 5. In principle, a single type-I quantum well structure can be formed with dilute-As GaNAs active region and GaN or AlGaN

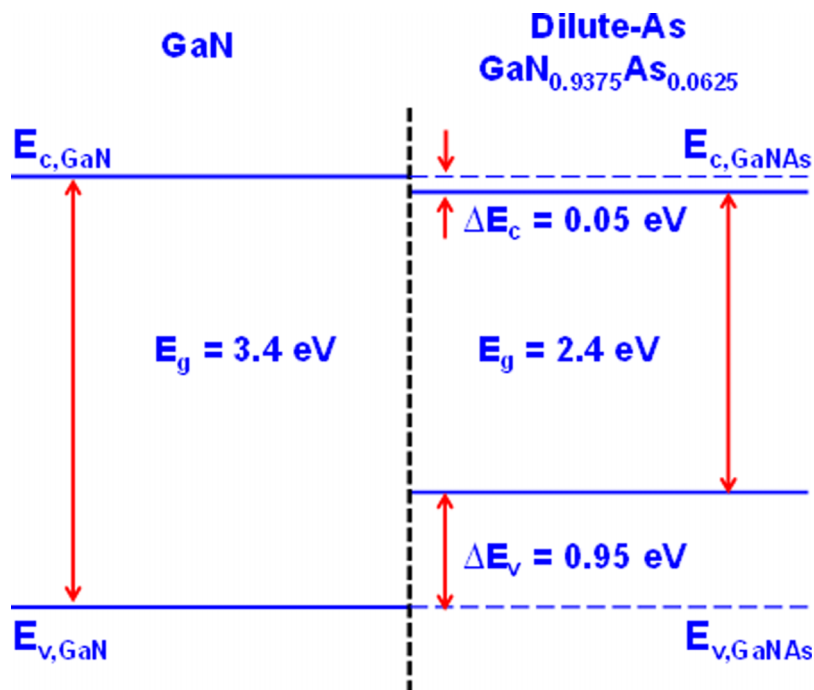


FIG. 5. Illustration of type-I band alignment of GaN / GaN<sub>0.9375</sub>As<sub>0.0625</sub> heterojunction based on the calculated conduction to valence band offset ratio.

barrier regions. The enhancement of the hole localization by using dilute-As GaNAs QW structure is expected to result in the increment of the exciton binding energy.<sup>35,43</sup> However, the use of GaN barriers will result in relatively weak electron confinement in the GaNAs QW. The use of AlGaIn tensile barriers<sup>44</sup> will potentially result in the strain compensation and improved barrier confinement in type-I GaNAs QW structure. In addition, the use of dilute-As GaNAs alloy had previously been suggested in type-II InGaIn / dilute-As GaNAs QWs<sup>27,28</sup> for addressing the charge separation issue in the QW. The use of dilute-As GaNAs with large valence band offset in type-II QW structure results in strong hole confinement, which in turn increase the electron-hole wavefunction overlap in polar InGaIn-based QWs resulting in improved spontaneous emission rate and optical gain.<sup>27,28</sup>

#### IV. CONCLUSIONS

In summary, the natural band alignment of dilute-As GaNAs / GaN heterostructure is determined via First-Principle method. Our finding shows a type-I natural band alignment of dilute-As GaNAs / GaN heterostructure, with the conduction to valence band offset ratio (CBO : VBO) determined as 5:95 for As-content up to 12.5%. The strong coupling of localized As-states is found as the primary contributing factor in leading to the strong valence band modification resulting in the bandgap reduction observed in the dilute-As GaNAs alloy. Future works on the impacts of the As-clustering in the dilute-As GaNAs with high As-content on its band alignment with respect to that of GaN will be important. The incorporation of dilute-As GaNAs alloy in the type-I or type-II QW structures can result in significantly improved active regions for LEDs and lasers emitting in the visible spectral regimes.

#### ACKNOWLEDGMENTS

The work was supported by US National Science Foundation (ECCS 1408051, ECCS 1028490, DMR 0907260), and the Daniel E. '39 and Patricia M. Smith Endowed Chair Professorship Fund. The authors also acknowledge helpful technical discussions with Dr. Hannes Schweiger from Material Design. The authors also would like to acknowledge useful discussions with Dr. Benjamin O. Tayo, Dr. Jing Zhang, and Dr. Guangyu Liu, all from Lehigh University.

- <sup>1</sup> S. Nakamura, *Science* **281**, 956–961 (1998).
- <sup>2</sup> M. H. Crawford, *IEEE J. Sel. Top. Quantum Electron.* **15**, 1028-1040 (2009).
- <sup>3</sup> H. Zhao, G. Y. Liu, J. Zhang, J. D. Poplawsky, V. Dierolf, and N. Tansu, *Optics Express* **19**, A991-A1007 (2011).
- <sup>4</sup> H. Zhao, G. Liu, R. A. Arif, and N. Tansu, *Solid-State Electronics* **54**, 1119–1124 (2010).
- <sup>5</sup> X. Li, S. Kim, E. E. Reuter, S. G. Bishop, and J. J. Coleman, *Appl. Phys. Lett.* **72**, 1990-1992 (1998).
- <sup>6</sup> X. Li, S. G. Bishop, and J. J. Coleman, *Appl. Phys. Lett.* **73**, 1179–1181 (1998).
- <sup>7</sup> X. Li, H. Liu, X. Ni, U. Ozgur, and H. Morkoc, *Superlattices and Microstructures* **47**, 118-122 (2010).
- <sup>8</sup> X. H. Li, R. Song, Y. K. Ee, P. Kumnorakaw, J. F. Gilchrist, and N. Tansu, *IEEE Photon. J.* **3**, 489–499 (2011).
- <sup>9</sup> I. H. Brown, P. Blood, P. M. Smowton, J. D. Thomson, S. M. Olaizola, A. M. Fox, P. J. Parbrook, and W. W. Chow, *IEEE J. Quantum Electron.* **42**, 1202–1208 (2006).
- <sup>10</sup> H. Zhang, E. J. Miller, E. T. Yu, C. Poblez, and J. S. Speck, *Appl. Phys. Lett.* **84**, 4644-4646 (2004).
- <sup>11</sup> P. K. York, K. J. Beernink, G. E. Fernandez, and J. J. Coleman, *Appl. Phys. Lett.* **54**, 499-501 (1989).
- <sup>12</sup> N. Tansu, J. Y. Yeh, and L. J. Mawst, *Appl. Phys. Lett.* **82**, 4038-4040 (2003).
- <sup>13</sup> K. Uesugi, N. Morooka, and I. Suemune, *Appl. Phys. Lett.* **74**, 1254-1256 (1999).
- <sup>14</sup> L. Xu, D. Patel, C. S. Menoni, J. Y. Yeh, L. J. Mawst, and N. Tansu, *Appl. Phys. Lett.* **89**, 171112 (2006).
- <sup>15</sup> H.-P. Komsa, E. Arola, E. Larkins, and T. T. Rantala, *J. Phys.:Condens. Matter* **20**, 315004 (2008).
- <sup>16</sup> N. Tansu, J. Y. Yeh, and L. J. Mawst, *IEEE J. Sel. Top. Quantum Electron.* **9**, 1220-1227 (2003).
- <sup>17</sup> S. R. Bank, L. L. Goddard, M. A. Wistey, H. B. Yuen, and J. S. Harris, *IEEE J. Sel. Top. Quantum Electron.* **11**, 1089-1098 (2005).
- <sup>18</sup> A. Lindsay and E. P. O'Reilly, *Phys. Rev. Lett.* **93**, 196402 (2004).
- <sup>19</sup> C. G. Van de Walle and J. Neugebauer, *Appl. Phys. Lett.* **76**, 1009–1011 (2000).
- <sup>20</sup> A. Kimura, C. A. Paulson, H. F. Tang, and T. F. Kuech, *Appl. Phys. Lett.* **84**, 1489-1491 (2004).
- <sup>21</sup> K. M. Yu, S. V. Novikov, R. Broesler, C. R. Staddon, M. Hawkridge, Z. Liliental-Weber, I. Demchenko, J. D. Denlinger, V. M. Kao, F. Luckert, R. W. Martin, W. Walukiewicz, and C. T. Foxon, *Phys. Status Solidi C* **7**, 1847–1849 (2010).
- <sup>22</sup> C. K. Tan, B. O. Tayo, J. Zhang, X. H. Li, G. Y. Liu, and N. Tansu, *J. Disp. Technol.* **9**, 272-279 (2013).
- <sup>23</sup> X. H. Li, H. Tong, H. P. Zhao, and N. Tansu, Proc. of the SPIE Photonics West 2010, Physics & Simulation of Optoelectronics Devices XVIII, **75970H** (2010).
- <sup>24</sup> T. Mattila and A. Zunger, *Phys. Rev. B* **59**, 9943-9953 (1999).

- <sup>25</sup> K. Laaksonen, H.-P. Komsa, E. Arola, T. T. Rantala, and R. M. Nieminen, *J. Phys.: Condens. Matter* **18**, 10097-10114 (2006).
- <sup>26</sup> J. Wu, W. Walukiewicz, K. M. Yu, J. D. Denlinger, W. Shan, J. W. Ager III, A. Kimura, H. F. Tang, and T. F. Kuech, *Phys. Rev. B* **70**, 115214 (2004).
- <sup>27</sup> R. A. Arif, H. Zhao, and N. Tansu, *Appl. Phys. Lett.* **92**, 011104 (2008).
- <sup>28</sup> H. Zhao, R. A. Arif, and N. Tansu, *J. Appl. Phys.* **104**, 043104 (2008).
- <sup>29</sup> M. Peressi, N. Binggeli, and A. Baldereschi, *J. Phys. D: Apply. Phys.* **31**, 1273-1299 (1997).
- <sup>30</sup> A. Baldereschi, S. Baroni, and R. Resta, *Phys. Rev. Lett.* **61**, 734-737 (1988).
- <sup>31</sup> L. Colombo, R. Resta, and S. Baroni, *Phys. Rev. B* **44**, 5572-5579 (1991).
- <sup>32</sup> N. R. D'Amico, G. Cantele, and D. Ninno, *Appl. Phys. Lett.* **101**, 141606 (2012).
- <sup>33</sup> P. G. Moses, M. Miao, Q. Yan, and C. G. Van de Walle, *J. Chem. Phys.* **134**, 084703 (2011).
- <sup>34</sup> P. G. Moses and C. G. Van de Walle, *Appl. Phys. Lett.* **96**, 021908 (2010).
- <sup>35</sup> L. Dong and S. P. Alpay, *J. Appl. Phys.* **111**, 113714 (2012).
- <sup>36</sup> S. H. Wei and A. Zunger, *Appl. Phys. Lett.* **72**, 2011-2013 (1998).
- <sup>37</sup> J. Robertson, *J. Vac. Sci. Technol. B* **18**, 1785-1791 (2000).
- <sup>38</sup> B. Hoffling, A. Schleife, C. Rodl, and F. Bechstedt, *Phys. Rev. B* **85**, 035305 (2012).
- <sup>39</sup> Material Designs Inc., Santa Fe, NM, USA, MedeA-VASP, <http://www.materialsdesign.com>.
- <sup>40</sup> V. Fiorentini and A. Baldereschi, *Phys. Rev. B* **51**, 11169-11186 (1996).
- <sup>41</sup> P. W. Peacock and J. Robertson, *Phys. Rev. Lett.* **92**, 057601 (2004).
- <sup>42</sup> I. Vurgaftman and J. R. Meyer, *J. Appl. Phys.* **94**, 3675-3696 (2003).
- <sup>43</sup> D. A. B. Miller, D. S. Chemla, T. C. Damen, A. C. Gossard, W. Wiegmann, T. H. Wood, and C. A. Burrus, *Phys. Rev. B* **32**, 1043-1060 (1985).
- <sup>44</sup> H. P. Zhao, R. A. Arif, Y. K. Ee, and N. Tansu, *IEEE J. Quantum Electron.* **45**(1-2), 66-78 (2009).